

# Parallel SPH modeling using dynamic domain decomposition and load balancing displacement of Voronoi subdomains

M. S. Egorova<sup>a,d</sup>, S. A. Dyachkov<sup>a,b,c,d</sup>, A. N. Parshikov<sup>a,c</sup>, V. V. Zhakhovsky<sup>a,d</sup>

<sup>a</sup>*Dukhov Research Institute of Automatics (VNIIA), Moscow, Russia*

<sup>b</sup>*Moscow Institute of Physics and Technology, Dolgoprudny, Moscow Region, Russia*

<sup>c</sup>*Joint Institute for High Temperatures of the Russian Academy of Sciences, Moscow, Russia*

<sup>d</sup>*Landau Institute for Theoretical Physics of the Russian Academy of Sciences, Chernogolovka, Moscow Region, Russia*

---

## Abstract

A highly adaptive load balancing algorithm for parallel simulations using particle methods, such as molecular dynamics and smoothed particle hydrodynamics (SPH), is developed. Our algorithm is based on the dynamic spatial decomposition of simulated material samples between Voronoi subdomains, where each subdomain with all its particles is handled by a single computational process which is typically run on a single CPU core of a multiprocessor computing cluster.

The algorithm shifts the positions of neighbor Voronoi subdomains in accordance with the local load imbalance between the corresponding processes. It results in a transfer of particles from heavy-loaded processes to less-loaded ones. Iteration of the algorithm puts into alignment the processor loads. Convergence to a well-balanced decomposition from imbalanced one is demonstrated in static tests with a material at rest.

The high adaptability of the balancing algorithm to simulation conditions is illustrated by SPH modeling of the dynamic behavior of materials under extreme conditions, which are characterized by large pressure and velocity gradients, as a result of which the spatial distribution of particles varies greatly in time. The higher parallel efficiency of our algorithm in such conditions is demonstrated by comparison with the corresponding static decomposition of the computational domain. Our algorithm shows almost perfect strong scalability in tests using from tens to several thousand processes.

*Keywords:* Voronoi dynamic domain decomposition, load balancing, particle methods, massive parallel computing

---

## 1. Introduction

The unsteady motion of materials in extreme conditions is characterized by significant pressure and velocity gradients, as well as the occurrence of free

---

*Email addresses:* egorova.maria.serg@gmail.com (M. S. Egorova), 6asi1z@gmail.com (V. V. Zhakhovsky)

surfaces and contact density discontinuities. Efficient parallel modeling of such motion encounters a problem of load balancing between computational resources in use. Algorithms using a static spatial decomposition of the computational domain cannot provide fair parallel efficiency, since the distribution of the workload, determined by the computational time required for calculating the motion, is not tied to the unsteady material flow. The existing load balancing algorithms discussed below are also inadequate to adapt to rapid changes in spatial distribution of material.

This work aims to develop a highly adaptable load balancing algorithm which can be utilized in a parallel program designed for multiprocessor computing clusters. The efficient program must be able to load available processors with useful work evenly and maximally, thereby ensuring the high parallel efficiency of hydrodynamics simulation of high-rate processes and high-speed motion produced in materials under extreme conditions. Such conditions are realized in impact on heterogeneous obstacles, shock wave propagation in mesostructures of porous material, and other challenging problems which call for efficient parallel codes.

Efficient parallel modeling of detonation of explosives with pores and/or inert additives, splitting and merging of droplets in high-speed flows, impact fragmentation of brittle materials and high-speed collision of bodies is also demanded. The computational challenge of simulating such processes can be naturally addressed by employing meshless particle methods, such as molecular dynamics (MD) and smoothed particle hydrodynamics (SPH) methods, implemented in efficient parallel programs.

To model the processes listed above the meshless SPH method [1] is preferable to the grid methods that encounter great difficulties in the exact resolution of shock fronts, contact surfaces and free boundaries (for the Euler formalism) and the construction of movable adaptive grids under the Lagrangian representation of continuum. In this paper a further description is based on our experience in developing a massively parallel program for the contact SPH method (CSPH) utilizing the Riemann solver [2] for interparticle interaction. However, an algorithm of dynamic domain decomposition described below is quite universal and can be applied not only for SPH, but it is suitable for any other particle method with a finite radius of interaction between particles; for example, for the direct Monte-Carlo, particle in cell (PIC) and MD methods.

The optimal distribution of computational loads between threads, computational processes or processor cores on a computing cluster is the cornerstone of efficient parallel program architecture. For the hydrodynamic modeling, the problem of load assignment reduces to a partitioning of samples, i.e., to the decomposition of simulated material in samples between computational processes. An even decomposition is necessary, but not a sufficient condition for optimality, since the data exchange between processes is determined by numbers of interacting particles that are found in different processes. These particles are distributed in the boundary layers between the processes if the spatial decomposition on subdomains among the processes is used. The exchange of information on boundary particles is required to support interaction between neighboring subdomains that belong to different processes.

As it is shown in [3], the spatial decomposition algorithms for MD method are optimal among other concepts of decomposition (in comparison with decomposition by particle numbers [3] or decomposition of a matrix of forces [4, 5]), as they allow not only to equalize the workload between processes, but also

to minimize the data exchange between them. An extensive data exchange, which is required in the decomposition by particle numbers for taking into account interaction of particles randomly distributed in the samples, does not allow achieving the high computational efficiency on large clusters with limited network bandwidth.

The most straightforward method of spatial decomposition is a partitioning of a computational domain into equal rectangular subdomains [6, 7]. In the context of spatial nonuniformity of particle concentration, the partitioning can be performed recursively, using the orthogonal recursive bisection (ORB) method. General issues of applying this approach to particle methods with a finite interaction radius were considered in [8], the specific case of its application to SPH was presented in [9, 10]. The idea of the technique is simple: a rectangular area is recursively divided into two parts along the long side so that an equal number of particles are found in each. The boundaries between rectangular subdomains are planes that are parallel to coordinate axes. Balancing is carried out via mobility of the planes separating those subdomains. But with re-balancing, the connectivity between processes can change significantly. Since subdomains have different numbers of neighbors, a reorganization of the decomposition requires the extensive particle exchanges. This decomposition method also does not take into account particle mixing during their motion. All this, taken together, increases the calculation time due to extensive particle data exchanges in the boundary layers between the processes.

An approach that uses decomposition based on rectangles generated not from a large scale to a smaller one like it is done by ORB, but from a small scale to a larger scale is also possible. The computational domain can be decomposed by a Cartesian grid into small cells, and the decomposition is performed by distributing the groups of microcells among the processes [11, 12]. Microcells of one process must form a simply connected region. Microcells can migrate between processes, but the connectivity of the macro-regions remains constant. Such a limitation is a significant drawback for our problems, where the particles can significantly change the spatial arrangement because the undesirable additional particle data exchanges between the processes are required due to the migration of microcells mentioned above.

The third, more complex type of decomposition is the generation of an auxiliary grid in the computational domain, the cells of which, together with the particles in cells, are distributed among the computational processes [13, 14]. Load balancing is possible throughout the mobility of grid nodes, the connectivity of which is usually assumed to be fixed. During the calculation, the grid nodes are shifted towards the “load center” of the cells that have this node in the vertex list. The load center is approximated, for example, by the center of mass of the cells containing particles. To save the grid structure, the global decomposition adjustment algorithm is used. The main disadvantage of this decomposition method in application to our problems is that the grid cells can become significantly deformed, which increases the exchange of particles due to the lengthening of the cell boundaries and growth of the contact surface of neighboring cells.

Many works were presented in an attempt to find the most efficient technology of particle redistribution. The procedure for updating the decomposition should be consistent with the load balancing data. It is stated [15, 16, 17] that the ideal decomposition algorithm must be of diffusion type: the computational

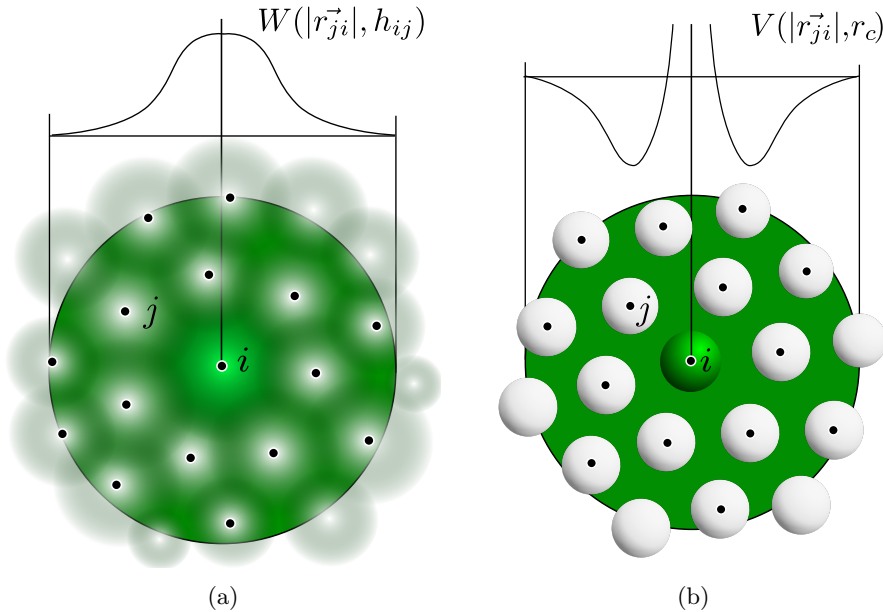


Figure 1: Interaction of the central particle  $i$  with neighboring particles  $j$  in SPH (a) and MD (b) methods. All calculations for the particle  $i$  are locally performed by summing up its interactions with the surrounding particles  $j$  in both SPH and MD. Such interaction is realized via the potential function in MD (b) or using the kernel function in SPH (a).

load should be redistributed in a manner similar to the heat conduction process. The workload is measured either proportionally to a number of particles in the computational subdomains [7, 10, 12], or, more naturally, by the time spent on computations [6, 8, 9, 18, 19]. The alternative method of balancing is performed not by the workload but by the cost of data transfer between subdomains [20], which does not guarantee the achievement of computational efficiency in the calculations.

The algorithm we propose is designed for massively parallel systems with distributed memory. It uses the idea of dynamic Voronoi decomposition [18, 19, 21], which is combined with some load auto-balancing algorithm. In accordance with [15, 16, 17], the load can be measured as a ratio of the useful calculation time to the total wall clock time required to accomplish a simulation step. We use this definition of load and adopt the method of load balancing for the Voronoi dynamic domain decomposition VD<sup>3</sup> initially proposed for MD method in [18].

Voronoi decomposition is uniquely defined by a set of generator points of the Voronoi diagram, where each point is associated with its cell and handled by a single process. The particles nearest to the Voronoi cell generator point are stored in memory and updated by a corresponding process. The mobility of the Voronoi diagram is realized through a mobility of the point generators because their positions are bound to movement of their own particles. The process load for each Voronoi cell can vary in time, which is caused by the following factors. First, the number of particles in the cell can vary due to algorithmic reasons (splitting and merging of particles, correction of the boundaries of the diagram due to displacements of the centers of the diagram), as well as to physical reasons including changes of density distribution and/or disruption

of the continuity in media surrounding generator point. Secondly, the physical processes inside all particle are local, and therefore can be calculated by their own algorithms for different times. The above factors lead to the fact that sets of SPH particles in each Voronoi subdomain are processed for different times, which means an uneven load of processes. Therefore, the positions of the point generators are further adjusted by a balancing displacement [18] resulting in particle transfer from heavily load cells to lesser load cells, which balances the process loads. Here, for the first time, this load auto-balancing algorithm for the VD<sup>3</sup> combined with the SPH method is implemented in our parallel SPH code, which is proved to be highly efficient in several tests.

The used auto-balancing algorithm for VD<sup>3</sup> makes it possible to take into account the redistribution of masses within a computational domain in a natural way during modeling. The algorithm is able to adapt to arbitrary mass flows with minimal exchange of particles between cells without requiring the preservation of connectivity between the diagram generators. The data exchange between pairs of processes/cells of the diagram is always local. The load balancing is fully adaptive, and it is not necessary to rebuild it from scratch to maximize the parallel efficiency of simulation. The cell boundaries through which the particle exchange is performed usually have less area than in the methods with block/rectangle decomposition of the computational domain.

The Voronoi decomposition with this load balancing does not have disadvantages typical for the decomposition methods listed above. Our computational experience shows that the geometry of cells tends to a honeycomb structure that has the minimum volume of cell boundary layers. It maximizes the loads by reduction of the number of particles to be exchanged. The Voronoi subdomains also tend to have an equal number of neighboring subdomains while the connectivity of subdomains is not fixed and can change following the material motion. The changes of the connectivity remain local in this case, that does not require massive communications between all processes because communications between subdomains are carried out only within the circle of the nearest neighborhood. Thus, despite the fact that the Voronoi decomposition is more difficult for programming than the methods mentioned above, it has undeniable advantages in the parallel modeling of complex flows triggered by extreme conditions.

## 2. Short-range particle methods

The Voronoi auto-balancing decomposition algorithm is suitable for any numerical method that represents material as a set of discrete objects interacting by short-range forces. Here we discuss two typical particle methods, MD and SPH, for which the short-range interatomic and interparticle interactions, respectively, allows to organize the particle data structures and data exchange among the Voronoi cells similarly.

As can be seen from Fig. 1, the geometry of particle interaction in MD system and SPH-medium is organized identically. In the MD medium, each atom exchanges energy and momentum only with its neighbors in the region of the interaction potential  $V(|\vec{r}_{ij}|, r_c)$ , where  $|\vec{r}_{ij}|$  is the distance between the particles and  $r_c$  is a cut-off radius of used interatomic potential. Likewise, each SPH particle interacts only with those particles that are within the smoothing kernel

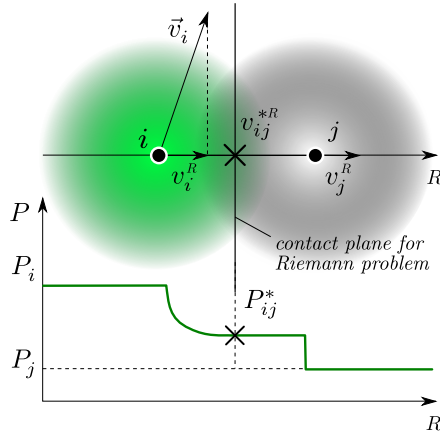


Figure 2: The contact SPH using the Riemann solver. Interparticle interaction is approximated by the Riemann problem solution at the contact between a pair of neighbor particles.

$W(|\vec{r}_{ij}|, h_{ij})$  of support area, where  $h_{ij}$  is a smoothing length between the particles  $i$  and  $j$ . The limited interaction radius makes it possible to take into account the interaction of SPH particles only within the Voronoi cell and with other cells' bordering particles in the zone determined by the radius of the smoothing kernel. In this case, load balancing can be efficiently performed by particle transfer between adjacent Voronoi cells.

Interaction of particles in CSPH [2, 22] is provided by the Riemann solver applied for each pair  $i - j$  of interacting particles  $i$  and  $j$ , as illustrated by Fig. 2. The velocity components  $v_i^R = \vec{v}_i \cdot \vec{e}^R$ ,  $v_j^R = \vec{v}_j \cdot \vec{e}^R$  of the particles  $i$  and  $j$  are used as left and right state velocities, where  $\vec{e}^R = (\vec{r}_j - \vec{r}_i)/|\vec{r}_j - \vec{r}_i|$  is a direction vector. Then, the velocity  $v_{ij}^{*R}$  and pressure  $P_{ij}^*$  can be obtained by the Riemann solver. CSPH-approximations of conservation laws can be found as:

$$\frac{d\rho_i}{dt} = 2\rho_i \sum_j \frac{m_j}{\rho_j} (v_i^R - v_{ij}^{*R}) \vec{e}^R \cdot \nabla_i W_{ij} \quad (1)$$

$$\frac{d\vec{v}_i}{dt} = -\frac{2}{\rho_i} \sum_j \frac{m_j}{\rho_j} P_{ij}^* \nabla_i W_{ij} \quad (2)$$

Here  $r_{ij} = |\vec{r}_i - \vec{r}_j|$ ,  $W_{ij} = W(r_{ij}/h_{ij})$  is a smoothing kernel between particles  $i$  and  $j$ ,  $h_{ij}$  — a smoothing length. The kernel gradient equals to  $\nabla_i W_{ij} = -\vec{e}^R W'_{ij}$ . Unlike [2], our code uses a conservative formulation of the energy conservation law:

$$\frac{dE_i}{dt} = -\frac{2}{\rho_i} \sum_j \frac{m_j}{\rho_j} P_{ij}^* v_{ij}^{*R} \vec{e}^R \cdot \nabla_i W_{ij} \quad (3)$$

Where the total energy  $E_i = e_i + v_i^2/2$  is the sum of the internal and kinetic energies of a unit mass in  $i$ -particle.

The high energy density physics usually addresses the problems where the SPH particles can contract or expand easily, so the variability of the smoothing length is significant. The particle size is defined as  $d_i = \sqrt[3]{m_i/\rho_i}$ . To ensure the pair

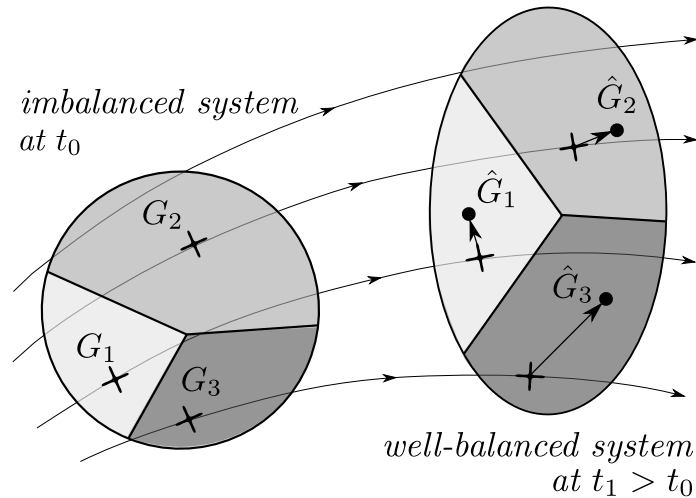


Figure 3: Displacement of the Voronoi generator for each subdomain is determined by a weighted sum of its material flow movement for a simulation step and balancing displacements for pairs with surrounding Voronoi subdomains to equalize the loads of the corresponding processes.

symmetry of interparticle interaction, it is necessary to specify the symmetric smoothing distance:

$$h_{ij} = (d_i + d_j) / 2. \quad (4)$$

The interaction distance of the particles depends on a chosen smoothing kernel, and generally  $W(r_{ij}/h_{ij}) > 0$  for  $|r_{ij}^{\vec{r}}| < \varkappa h_{ij}$ , where  $\varkappa$  is a radius of smoothing kernel. All results presented in Section 5 are obtained using the Wendland kernel  $C^2$  [23] with the radius of  $\varkappa = 1.936$ .

### 3. Autobalancing Voronoi dynamic domain decomposition

#### 3.1. Voronoi domain decomposition

The Voronoi diagram according to [24] is a decomposition of a closed subspace  $\bar{\Omega} \in \mathcal{R}^n$  (a modeled volume or a computational domain in an  $n$ -dimensional space) between  $N_{\hat{V}}$  regions  $\{V_k\}_{k=1}^{N_{\hat{V}}}$  based on distance to a specific set of Voronoi generators  $\{G_k\}_{k=1}^{N_{\hat{V}}}$  points:

$$\hat{V}_k = \{\vec{x} \in \Omega : |\vec{x} - \vec{g}_k| < |\vec{x} - \vec{g}_l|, l = 1, \dots, N_{\hat{V}}, l \neq k\}, \quad (5)$$

where  $\vec{g}_k$  is a radius-vector of the point  $G_k$ . The definition (5) states that a single Voronoi subdomain is a convex polytope which contains all points that are closest to its generator with respect to any other generator. The Voronoi diagram is unique for a given set  $\{G_k\}_{k=1}^{N_{\hat{V}}}$ .

Suppose there is a material sample or a set of samples represented by particles in a computational domain, and a job with  $N_p$  parallel processes can be submitted on a computing cluster. Let each  $k$ -process operates one Voronoi subdomain  $\hat{V}_k$ . A set of generator points  $\{G_k\}_{k=1}^{N_p}$  can be placed someway in this domain, and a peer-to-peer connection between running processes  $k = 1, 2, \dots, N_p$

is established. Then all particles of the samples can be assigned to different processes according to the particle positions. That is the data structures describing particles in the subdomain  $\hat{V}_k$  is stored in the memory of the process  $k$ . If a particle locates exactly on a boundary between  $\hat{V}_k$  and  $\hat{V}_l$ , then it is associated with the subdomain  $\hat{V}_{\min\{k,l\}}$ .

The VD<sup>3</sup> algorithm proposed in this paper allows a generator to move following the local material flow of the particles assigned to the corresponding subdomain, while the balancing algorithm corrects the displacements of generators to achieve a load balance between subdomains (i.e., between the corresponding processes), as it was done for the MD in [18] and is illustrated by Fig. 3. Once the new boundaries for new generator positions are found, new assignment of particles is realized by sending all particles located beyond the boundaries to corresponding subdomain/process using the definition (5).

The information only about neighboring Voronoi subdomains, that are located within lookup radius  $R_k > |\vec{g}_k - \vec{g}_l|$ ,  $l \neq k$ , is required for  $\hat{V}_k$  to organize a proper particle re-assignment. By exchanging particles with all adjacent subdomains/processes, the  $\hat{V}_k$  gets all the particles located within its boundaries and gives away all that are not. Using the distance  $R_k$  for determining the subdomain neighborhood is necessary because a mixing of subdomains is expected and Voronoi diagram connectivity may change. To reduce the number of inter-process communications it is appropriate to choose  $R_k$  large enough to ensure that all neighbors are listed.

The accuracy of simulation in a large computational domain, where particle coordinates vary in several orders of magnitude, is subjected to truncation errors in the calculation of interparticle distances. To reduce these errors, the different local coordinate systems for each Voronoi subdomain  $\hat{V}_k$  are used instead of a global computational domain system. A good choice for an origin of a local coordinate system is a geometrical center of  $N_k$  particles inside domain:

$$\vec{r}_{c,k} = \frac{1}{N_k} \sum_{i=1}^{N_k} \vec{r}_i. \quad (6)$$

Then the values of particle coordinates are restricted by subdomain dimensions. However, the truncation errors may appear if this center moves with particles and also after particle transfer between different subdomains. To avoid the effect of coordinate system change the origins of local systems are assigned to the nearest mesh site in which the mesh size equals the unit of length in use. Thus, the coordinate of a particle experiences occasionally an integer shift without truncation error, when the origin obtains a new mesh position or the particle is transferred between subdomains. Generator coordinates are not rounded to the mesh size, i.e., they remain in the global computational domain system.

### 3.2. Load balancing by displacement of generators

Once all particles of simulated samples are distributed among the processes following the Voronoi diagram, simulation of particle motion starts. Each process that handles particles is hereinafter called as a worker. Preparation of neighbors list and calculating the interaction of particles are necessary parts in any particle method implementation, so their execution should be considered as a useful work utilized locally by each computational process/worker.



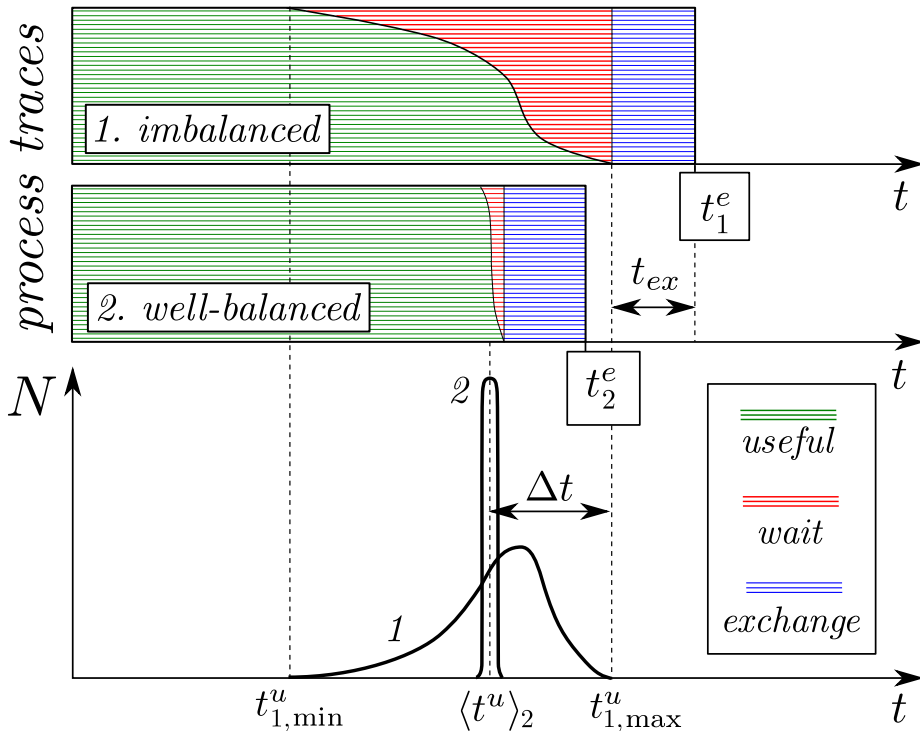


Figure 4: The schematic traces (1 and 2) of the parallel processes arranged by the useful times utilized for specific SPH calculations, shown by green lines, within a simulation step and the corresponding distributions of the number of processes as functions of the useful time. Load balancing 1  $\rightarrow$  2 leads to a narrower distribution, which in turn results in shorter waiting times and faster simulation. Here the sum of useful times and exchange times spent by all processes is assumed fixed for simplicity. In real conditions, the exchange times are usually reduced with balancing.

However, the parallel algorithms have to carry out additional work on data exchange. Having an efficient useful part controlled essentially by a total number of particles, the simulation performance can be improved only by minimizing the elapsed wall clock time.

Let  $t^e$  be the elapsed time spent on one simulation step. It can be easily counted by a program and is determined by the barrier synchronization between the worker processes to obtain the shortest duration of a next simulation step. That is the workers cannot proceed to the next step until all workers complete the current step. This unavoidable synchronization allows us to state that  $\forall k : t_k^e = t^e$ .

It is also easy to measure the useful time  $t_k^u$  spent by a worker  $k$  to process the particle interaction during one simulation step. The remaining time  $t_k^x$  is determined through the difference between the elapsed time per step  $t^e$  and the useful time:

$$t^e = t_k^u + t_k^x. \quad (7)$$

In general, the time  $t_k^x$  can be split into idle time, or waiting time,  $t_k^w$  and exchange time  $t_k^{\text{ex}}$ :

$$t_k^x = t_k^{\text{ex}} + t_k^w, \quad (8)$$

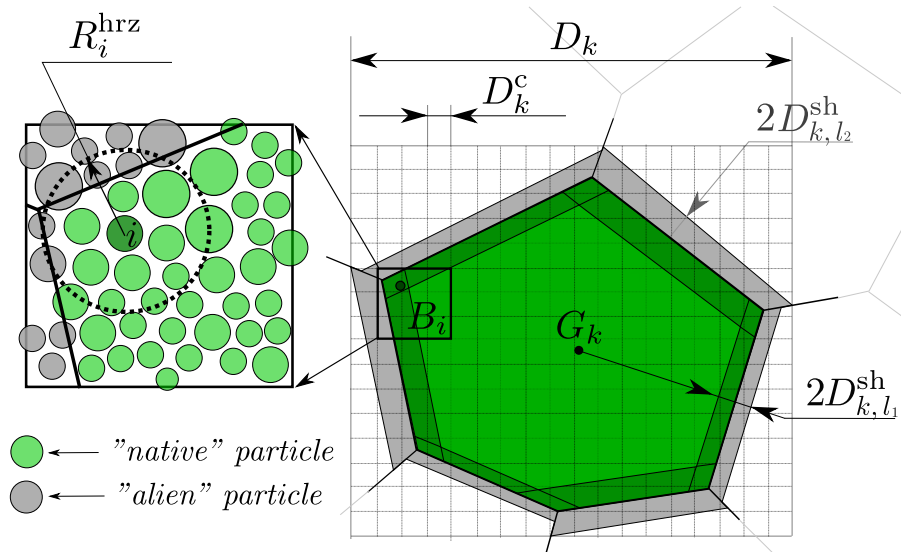


Figure 5: A uniform cubic lattice with cell size  $D^c$  is constructed in a Voronoi subdomain corresponding to the generator point  $G_k$ . The green-colored Voronoi subdomain is surrounded by the gray zone that belongs to the neighbor subdomains. Zone width and alien particles within are synchronized with the neighbor subdomains at a neighbor list update. The darker green area is a part of Voronoi subdomain  $V_k$ , information about which the process  $k$  provides to its neighbors. The area  $B_i$  of the linked list for the SPH particle  $i$  is shown in the left inset.

where the waiting time is mostly resulted from the not equal useful times of workers, i.e. the load imbalance. But in practice, it is difficult to determine which time is spent for waiting of data transfer, and which for data exchange itself, especially if non-blocking communications are used. The use of nonblocking communications makes it possible to mask partially the waiting time for data transfer of copies of particles from the boundary layers: while the  $k$ -th process is waiting for the “alien” particles from the  $l$  process, calculation of interaction of “natives” with “natives” either in  $k$  or in  $l$  can be performed (see section 3.3).

Thus, the parallel modeling efficiency of a worker  $k$  can be characterized by a load ratio:

$$L_k = \frac{t_k^u}{t_k^e}, \quad 0 < L_k < 1, \quad (9)$$

which is called as a load of worker  $k$ .

Sometimes several programs executed simultaneously may compete for CPU resources. Nevertheless, it is usually possible to count the processor-dependent time which CPU has exclusively spent on execution of a particular scalar code. The useful work, which is the most resource intensive part, is then may be counted in both ways: as the elapsed useful time  $t^u$  and useful CPU-time  $t_{\text{CPU}}^u$ . The fraction  $f^p = t_{\text{CPU}}^u/t^u$  defines the available computational capability. It can be used to improve the definition of worker load in a competitive execution environment as:

$$L_k = \frac{t_k^u}{f_k^p t_k^e}. \quad (10)$$

This formula can be also applied to take into account the different capabilities of various CPUs in use, say in computational grid environments [18].

Our goal now is to develop an algorithm that maximizes the average load of  $N_p$  used workers:

$$\langle L \rangle = \frac{1}{N_p} \sum_{k=1}^{N_p} L_k. \quad (11)$$

The entire amount of useful work is almost fixed and determined by a total number of particles involved into particular simulation, so the average useful time  $\langle t^u \rangle$  does not depend on the distribution of SPH particles among processes. However, the entire work can be highly nonuniformly distributed, which leads to a large gap between  $t_{\max}^u = \max_k \{t_k^u\}$  and  $\langle t^u \rangle$ , as shown in Fig. 4. A similar gap exists in the load distribution:

$$\Delta L = L_{\max} - \langle L \rangle, \quad (12)$$

so the well-balanced load is achieved at minimization of this gap. The importance of load balancing is that by reducing  $\Delta L$ , the average load can be increased and the wall clock simulation time is reduced. To do this, it is necessary to transfer particles from heavily loaded processes to less loaded ones to make the distribution of the number of processes over the useful time narrower, as illustrated by Fig. 4.

To illustrate that reduction of the imbalance leads to decrease of simulation time, we consider the following example. It is assumed that the program runs on a clean homogeneous computing cluster without other competing tasks, so  $f_k^p = 1$ . Denoting  $\Delta t = t_{\max}^u - \langle t^u \rangle$  and assuming that the deviations of  $t_k^{\text{ex}}$  from the mean time of data exchange  $t^{\text{ex}} = \sum_k t_k^{\text{ex}}/N$  are small, the average load can be expressed as:

$$\langle L \rangle = \frac{\langle t^u \rangle}{\langle t^e \rangle} = \frac{\langle t^u \rangle}{\langle t^u \rangle + \Delta t + \langle t^{\text{ex}} \rangle}. \quad (13)$$

The formula (13) is illustrated by Fig. 4. Further, one can find

$$\Delta t = \frac{\langle t^u \rangle}{\langle L \rangle} \left( \frac{t_{\max}^u}{\langle t^u \rangle} \langle L \rangle - \langle L \rangle \right) = \frac{\langle t^u \rangle}{\langle L \rangle} \Delta L, \quad (14)$$

which, combined with (13), gives

$$\langle L \rangle = \frac{\langle t^u \rangle}{\langle t^u \rangle + \langle t^{\text{ex}} \rangle} (1 - \Delta L). \quad (15)$$

It is now clear that the average efficiency of modeling increases with reduction of the gap between the heavily loaded workers and the average loaded ones. However, an ideal balance ( $\Delta L = 0$ ) does not guarantee a perfect efficiency: it is necessary to reduce  $t^{\text{ex}}$ , which depends on the number of particles to be exchanged, as well as on the bandwidth and network delays, which is not the aim of this work. However, the time  $t^{\text{ex}}$  is significantly reduced by the data exchange masking with non-blocking communications used in our code.

Our strategy of load balancing is to use a vector sum of Voronoi generator shifts which linearly depend on pairwise load imbalance:

$$\Delta \vec{g}_k = \sum_{l=1}^{M_k} D_{k,l}^{\text{sh}} \frac{L_k - L_l}{L_k + L_l} \frac{\vec{g}_{kl}}{|\vec{g}_{kl}|}, \quad (16)$$

where  $D_{k,l}^{\text{sh}}$  is a width of boundary layer, or an exchange shell of the Voronoi subdomain  $\hat{V}_k$  shown on Fig. 5,  $M_k$  is a number of surrounding Voronoi subdomains for  $\hat{V}_k$ . If  $\Delta\vec{g}_k = 0$  is set for all  $k$ , there are no balancing displacements and Voronoi subdomains move following their particles.

To realize the different types of spatial decompositions a new position  $\hat{g}_k$  of  $k$ -generator can be defined as a weighted summation of its Lagrangian movement of the particles within  $\hat{V}_k$  during some time interval and a balancing displacement  $\Delta\vec{g}_k$  as follows:

$$\hat{g}_k = (1 - \theta)(\vec{g}_k + \Delta\vec{g}_k) + \theta(\vec{r}_{c,k} + \Delta\vec{r}_{c,k}), \quad (17)$$

where  $\vec{g}_k$  is a previous position of the generator,  $\vec{r}_{c,k} + \Delta\vec{r}_{c,k}$  are previous Lagrangian position plus its movement, and  $\theta \in [0, 1]$  is a parameter specifying whether the Voronoi subdomain movement is preferably determined by the Lagrangian movement (6) or by the load balancing mechanism (16). A simplified diagram shown in Fig. 3 illustrates such linear combination of Lagrangian movement and balancing displacement. If  $\theta = 1$  a new position of generator is fully determined by an actual geometric center  $\vec{r}_{c,k}$  of particles in  $\hat{V}_k$ . Then the evolution of VD<sup>3</sup> is exclusively controlled by the material motion. The choice of  $\theta = 0$  is inadequate to simulation of material motion and leads to large subdomain jitter resulting in extensive data exchange overheads. Static spatial decomposition is realized by  $\theta = 0$  and  $\Delta\vec{g}_k = 0$ . The  $\theta = 0.25$  is used in test modelings that we discuss below in Sections 4 and 5.

The presented load balancing strategy results in that a heavy-loaded worker attracts less-loaded neighbors and distributes its excess particles among them. The process is running iteratively, reducing the communication wait time and achieving the better parallel efficiency step by step. To reduce the computational overheads for re-balancing at each simulation step, the load balancing algorithm is executed once per a time interval consisting of  $N_{upd}$  simulation steps in our code. During this interval, the particles are not allowed to be transferred between subdomains.

### 3.3. Neighbor particle lists used in Voronoi subdomains

For the direct search of neighboring particles, the  $\mathcal{O}(N)$  operations are required to find all particles  $j$  interacting with a chosen central particle  $i \in [1, N]$ . The search for all interacting pairs requires  $\mathcal{O}(N^2)$  operations. Given the finite interaction radius, the number can be reduced to  $\mathcal{O}(N)$  using a list of neighbor particles.

Generation of a neighbor list for particles within each Voronoi subdomain takes a considerable amount of time. Moreover, the neighbor list which includes “alien” particles from adjacent boundary layers with each surrounding Voronoi subdomains is required to find all neighbor particles. To reduce the computational overheads for neighbor list generation the list can be updated once in several time steps by utilizing the Verlet approach [25]. The idea is that neighbors of an individual particle are considered within a sphere which includes not only interacting particles but also ones in a buffer shell with a large enough horizon radius  $R^{\text{hrz}}$  which is larger than an interaction radius. During several simulation steps this buffer may provide particles for the further interaction without update of the neighbor list. Such an enhanced neighbor list is called as the Verlet list (VL). The “alien” particles are also included in the VL for several

---

**Algorithm 1** Data exchange and decomposition update after  $N^{\text{upd}}$  simulation steps

---

```

1: procedure
2:     ▷ /*Update Voronoi decomposition for all k-processes*/
3:     Make balancing shift  $G_k$  using Eq. (17) from section 3.1.
4:     Reassign particles between  $\hat{V}_k$  and its neighbors  $\hat{V}_l$  using definition (5)
       from section 3.1.
5:     Calculate exchange layer width  $D_{k,l}^{\text{sh}}$  from Eq. (21) from section 3.4.
6:     Send lists of “native” particles in the exchange boundary layers to  $\hat{V}_l$ .
7:     Obtain lists of “alien” particles in the exchange layers from neighbors
        $\hat{V}_l$ .
8:     Build two separate Verlet lists for “native” and “alien” particles in  $\hat{V}_k$ .
9:     ▷ /*Perform next  $N^{\text{upd}}$  simulation steps*/
10:    for  $i = 1$  to  $N^{\text{upd}}$  do
11:        request for information about “alien” particles.
12:        do SPH calculations of interaction between “native” particles and
       “natives”.
13:        get information about “alien” particles.
14:        do SPH calculations of interaction between “native” particles with
       “aliens”.
15:        renew particle positions and states and make global synchronization
       of SPH time step.
16:        count the useful time  $t_k^{\text{u}}$ 
17:    end for
18:    count the elapsed time  $t_k^{\text{e}}$  to evaluate a new load  $L_k$ , and repeat this
       procedure.
19: end procedure

```

---

steps  $N^{\text{upd}}$  between the list updates. The list of neighbors is updated after each rebalancing of Voronoi decomposition, when boundary layers may change and the transfer of particles between the processes is allowed.

The efficiency of using the VL depends much on the buffer size and number of simulations steps which may proceed without the list update. In compressible SPH it is convenient to consider neighbors of a particle  $i$  in the individual sphere of the horizon radius  $R_i^{\text{hrz}} = R_i^{\text{int}} + R_i^{\text{buf}}$ , where  $R_i^{\text{int}}$  is a maximal local interaction distance,  $R_i^{\text{buf}} = \beta R_i^{\text{int}}$  is a buffer size with the parameter  $\beta > 0$ . If the buffer size is too small ( $\beta \rightarrow 0$ ) the neighbor list must be constructed at each simulation step to be sure that interparticle interaction is calculated properly. The number of neighbors within  $R^{\text{hrz}}$  grows as  $(1+\beta)^3$ , thus a larger  $\beta$  results in greater memory consumption and necessity to check distances with very many particles at each step that also increases computing time. Then an optimal  $\beta$  and a number of steps between updates  $N^{\text{upd}}$  can be found in a few trial tests. We use  $N^{\text{upd}} = 10 \div 15$  and  $\beta = 0.3 \div 0.6$  depending on specific simulation scenario.

To avoid calculation of  $\mathcal{O}(N_k^2)$  interparticle distances in order to construct the VL, all particles are associated with cubic cells of a mesh, which covers a Voronoi subdomain together with its “alien” particles in surrounding boundary layers as shown on Fig. 5. The two biggest particles with diameters  $d_1^{\text{max}}$

and  $d_2^{\max}$  should be found in the Voronoi subdomain and boundary layers to define the cell size  $D^c$

$$D^c = \frac{1}{2}(1 + \beta)\varkappa(d_1^{\max} + d_2^{\max}). \quad (18)$$

where  $\varkappa$  is determined in section 2. Such cell size definition guarantees that all native and alien neighbors of a central particle are allocated within  $3^3 = 27$  cells around it. This region is denoted as  $B_i$  in Fig. 5.

Indices of particles within all cells of the mesh are stored in a linked list (LL) having a form of integer vector, which size is equal to number of all  $N_k$  particles within a given Voronoi subdomain. To keep entry indices for LL a 3D integer array with dimensions corresponding to the mesh is allocated. If a cell is not occupied by particles the corresponding element of this 3D array is marked as zero. Otherwise, the index of first particle found in each cell is stored in the 3D array. This index points to the address of LL element where a next particle index in the same cell is allocated, as it is described in [25]. This linked procedure continues until the particle index points to a LL element containing zero, which ends the particle list for the cell. Using the linked list, the Verlet list can be generated performing  $\mathcal{O}(N_k)$  calculations of distances between particles located only in surrounding  $3^3$  cells.

A list of particles within  $B_i$  obtained from the LL is used to determine the maximal interaction distance  $R_i^{\text{int}}$  for  $i$ -particle as follows:

$$R_i^{\text{int}} = \frac{1}{2}\varkappa\left(d_i + \max_{j \neq i \in B_i} d_j\right), \quad (19)$$

and then the horizon radius is given:

$$R_i^{\text{hrz}} = (1 + \beta)R_i^{\text{int}}, \quad (20)$$

which is definitely smaller than  $D^c$  from Eq. (18). Such extended lists of neighbor particles for all  $B_i$  are used to build the VL containing only neighbors indices of particles which are placed within  $R_i^{\text{hrz}}$ .

Since modern computing systems have several levels of the memory hierarchy (from fast low-level CPU cache to slow RAM), simulation can be accelerated by increasing the probability of cache hits. To do so the particles, which spatially close to each other in simulation domain, should have the closer addresses in a linear RAM space. Then the calculation of their interactions is likely to be executed with using particle coordinates allocated in fast CPU cache. To utilize this idea the re-numbering and memory reallocation of neighbor particles using the Verlet list is performed from time to time. This procedure helps to decrease the cache missing rate, which is specifically amplified by extensive particle exchange between Voronoi subdomains, and thus provides a speedup up to 2 times with respect to a simulation in which such memory reordering of particles is not used.

#### 3.4. Adjusting interprocess data exchange for SPH

It is clear that the minimal width of boundary layer should be chosen to include all interacting particles near the boundary between Voronoi subdomains. As soon as we use the Verlet neighbor list it is necessary to acquire information about “alien” particles within a surrounding lookup area at every time

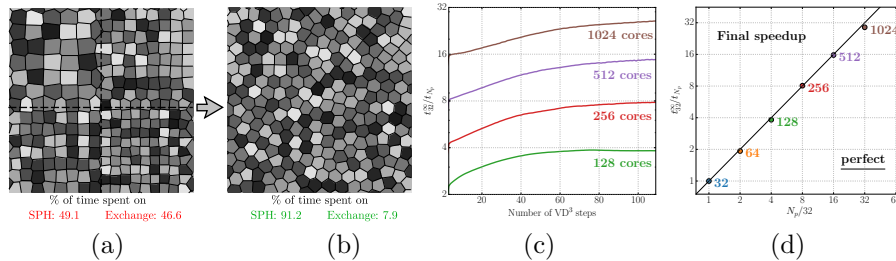


Figure 6: Stationary thin plate of sizes  $L_x = L_y = 1$  m,  $L_z = 0.15$  m consisting of 52 millions of particles is used for static tests of  $VD^3$  and autobalancing algorithm. Tests run on 32, 64 128, 256, 512, 1024 CPU cores with initial imbalance introduced into system. Fig. (a) shows initial imbalanced Voronoi diagram, where one quarter of the sample consists of  $N_p/8$  Voronoi subdomains, one consists of  $3N_p/8$  and two—of  $N_p/4$ . Transition from initial to well-balanced decomposition with 256 cores is demonstrated on the Figs. (a) and (b). Increase of speedup with iterations in transition from unbalanced to balanced decomposition is shown in the Fig. (c). Elapsed time per a step in well-balanced system is denoted as  $t^\infty$ . Final speedup as a function of CPU core number is almost linear for well-balanced decomposition as shown in the Fig. (d).

step. Then for all pairs of contacting Voronoi subdomain  $k$  and  $l$  the width of boundary layer  $D_{k,l}^{sh}$  must be determined. Using the maximal horizon radii in the Voronoi subdomains  $\hat{V}_k$  and  $\hat{V}_l$  we determine a layer width  $D_{k,l}^{sh}$  in a symmetric pairwise form as follows:

$$D_{k,l}^{sh} = \max \left[ \max_{i \in \hat{V}_k} R_i^{hrz}, \max_{i \in \hat{V}_l} R_i^{hrz} \right]. \quad (21)$$

That definition guarantees that the buffer zone with horizon radius  $R_i^{hrz}$  for each particle near the boundary is correctly filled with the “alien” particles. It is required to generate the identical lists of interactive “native–alien” particle pairs in both contacting Voronoi subdomains.

The boundary layer width (21) is then directly linked to the particles buffer size  $R^{buf}$ . By varying parameters  $\beta$  and  $N^{upd}$ , one may get not only optimal neighbor list length but also minimize the amount of data transfers and reduce both the exchange and elapsed times. It is possible to develop an algorithm for dynamic adjustment for  $\beta$  and  $N^{upd}$  during simulation aiming to reduce the elapsed time depending on simulation conditions, but this question is beyond the scope of this paper.

It should be noted that each process associated with Voronoi subdomain does not calculate “alien–alien” interaction. It receives the updated particles lists from its subdomain neighbors at each simulation step and handles only “native–native” and “native–alien” interactions. The code for these two parts can be executed separately, that provides the opportunity to mask waiting for “alien” particles by using asynchronous non-blocking MPI-communications and get them during calculation of “native–native”.

The pseudocode listed in Algorithm 1 summarizes all parts of the  $VD^3$  and the auto-balancing algorithm described in the above subsections of this section 3.

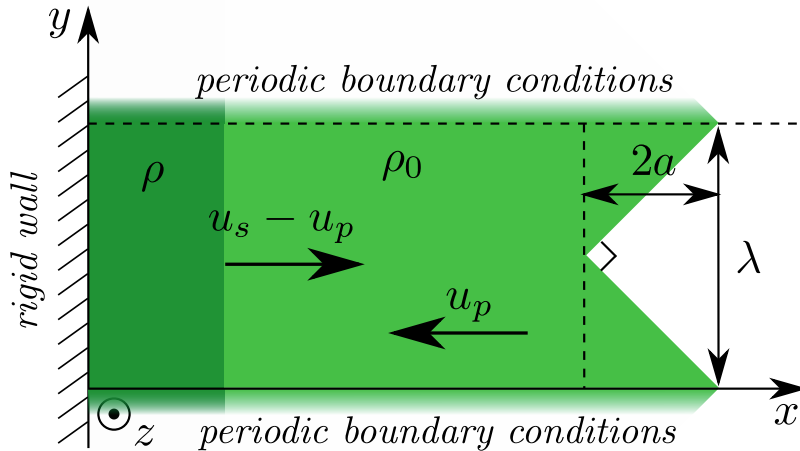


Figure 7: Geometry of lead sample used in simulation of ejecta from a grooved surface. PBC are imposed along  $y$ - and  $z$ -axes. Impact on a rigid wall with an initial particle velocity  $-u_p$  generates a shock wave propagating with velocity  $u_s - u_p$  in the chosen reference system toward the grooved surface.

#### 4. Parallel performance in static tests

The primary goal of the VD<sup>3</sup> with load balancing algorithm is to reduce a wall clock time required for simulation of nonuniform flow of materials. But first we have to check the strong scalability of VD<sup>3</sup> in static tests where material stays at rest all the simulation time, and only the number of CPU cores and positions of Voronoi generators can change. That allows testing the strong scalability in ideal conditions, without an effect of material motion on the realignment of decomposition. Dynamic testing the adaptive behavior of the algorithm under conditions of high-rate mass redistribution is discussed in the next Section 5.

The static tests with a steady sample are performed to trace the rearrangement of the initial decomposition to a well-balance one using the balancing algorithm and the dependence of calculation speedup on a number of processes involved. 2D decomposition is applied to a quasi-two-dimensional sample for clarity of decomposition visualization. A thin square plate of material with sizes  $L_x = L_y = 1$  m,  $L_z = 0.015$  m is considered at rest. The periodical boundary conditions (PBC) are imposed along all axes. The material is represented by about 52 millions of SPH particles. The number of particles remains constant in all static tests in order to check the strong scalability of our code, that is, the growth of calculations speedup with the increase of CPU cores  $N_p$  involved in decomposition.

Initially the load imbalance is introduced to the system by splitting each quarter of square sample by Voronoi subdomains in proportions  $3N_p/8$ ,  $N_p/4$ ,  $N_p/4$ ,  $N_p/8$  of total  $N_p$  MPI-processes as shown on Fig. 6(a). To initiate the decomposition rearrangement inside those quarters, small random shifts to initial Voronoi generator positions were applied. Due to memory limitation in a computing node of the used computing cluster,  $N_p$  is only varied from 32 to 1024.

Initial imbalance results in that almost half of the elapsed simulation time is spent on waiting for heavily loaded processes handling  $N_p/8$  Voronoi subdo-



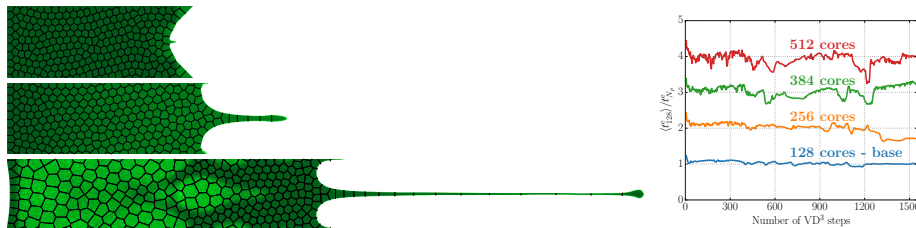


Figure 8: Maps of Voronoi subdomain boundaries and mass distributions in ejecta obtained in simulation using the  $VD^3$  on 256 processors is shown on the left, where the darker blue color corresponds to higher particle density. The relative speedups  $\langle t_{128}^e \rangle / t_{N_p}^e$  as functions of simulation step in modeling the same problem with 128, 256, 384, and 512 cores are presented on the right. Averaged elapsed time per step in modeling with 128 cores ( $t_{128}^e$ ) is used for evaluation of the relative speedup.

mains to accomplish their useful calculations. That involves Voronoi generators of less loaded subdomains into movement toward the adjacent heavy loaded ones, which leads to transfer of particles among them. After some balancing iterations, the decomposition reaches a well-balanced geometry. At this moment both the waiting time for communication between the neighboring Voronoi subdomains and the elapsed time per a simulation step reaches their minima (Fig. 6, b). In such state, the numbers of particles in all subdomains are almost equal.

Figure 6, (c) shows the evolution of the calculation speedup defined as a ratio of the wall clock elapsed time  $t_{128}^e$  per a step in a well-balanced final decomposition with 128 processes to the elapsed times measured during simulations using from 128 to 1024 processes. It is clear that the converging to a well-balanced state takes more iterations for a larger number of  $N_p$ . The reason is that two types of Voronoi subdomains are initially generated in the test: those located near the boundary between the quarters where they are subjected to significant load imbalance with subdomains from other quarters, and the subdomains located inside each quarter, which are in a good balance with surroundings. For a larger number of  $N_p$ , a ratio of the boundary subdomains to the inner ones becomes smaller, and more iterations are required to involve the internal subdomains in the balancing process.

It is worth to note that the Voronoi subdomain shapes transform to hexagonal during load balancing. It is because the hexagon has the lowest number of neighbors and a ratio of its perimeter to area is the smallest among regular polygons, which allows to minimize the number of alien particles in boundary layers and thereby to reduce data transfer and communications between subdomains.

Final speedup that is shown in Fig. 6(d) is measured for well-balanced decompositions with using 128, 256, 512, and 1024 CPU cores. One can notice, that the speedup is almost linear up to 1024 cores. Final deviation from the perfect linear speedup for 1024 cores is caused by the increased ratio between the time required for data exchange and the useful time for particle simulation. The reason for it is the growth of particle numbers in boundary layers between subdomains, which leads to a growth of data exchange per a simulation step. With the increase of boundary layer area and the corresponding decrease of inner area of subdomains, the data exchange masking by “natives”–“natives” calculations get less efficient with  $N_p$ .

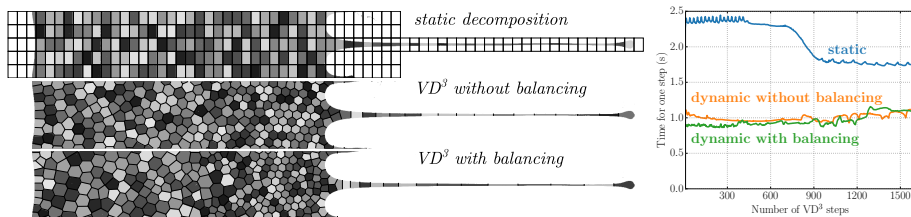


Figure 9: Maps of subdomain boundaries obtained in simulations of ejecta on 256 cores using the static rectangular decomposition, dynamic Lagrangian without balancing and  $VD^3$  with load balancing, from left to right respectively. Shades of gray are used to distinguish different subdomains only. The right plot shows the corresponding elapsed times per a step during simulation.

## 5. Parallel performance in dynamic tests with materials in extremes

In this section, the performance of auto balancing algorithm is checked in the modeling of complex material motion produces by extreme conditions, which leads to high-rate deformations and discontinuities in material, and thereby inhomogeneous spatial distribution of particles. In order to demonstrate the obtained results two-dimensional rather than three-dimensional Voronoi decomposition is used as in the previous section.

For the first dynamic test of the auto-balancing algorithm, the ejection from a rough metal surface produced by shock wave arrival is chosen [26, 27, 28, 29]. Surface grooves on metal may have small sizes of the order of 10–100  $\mu\text{m}$  depending on experimental setup. After reflection of a flat shock from such surface, the microscopic cumulative jets are formed, which may move with a speed of several km/s.

An explosion of a metal wire caused by fast energy deposition through the ohmic heating is considered in the second dynamic test. The magnetic field produced by a high current flowing in the wire keeps it from thermal expansion. The external magnetic pressure is balanced by the equal internal pressure of several GPa until the current cutoff. Heating is accompanied by wire material evaporation increasing with temperature growth. At some moment the electric electrical breakdown of surrounding vapor happens, which results in switching of the current into the coronal plasma. After the current cutoff in a wire, the magnetic pressure disappears, and the high-pressure material of wire begins to expand freely. To perform an SPH simulation test for this expansion stage only, we use the initial conditions provided by magnetohydrodynamic modeling of aluminum wire [30].

Tremendous deformation and fragmentation of samples, observed in experimental conditions discussed above, challenges the adaptability of any load-balancing algorithm with domain decomposition.

To close the system of equations (1)–(3), the well-known Mie–Gruneisen equation of state is used to model materials in extreme states:

$$P - P_r(\rho) = \Gamma\rho[e - e_r(\rho)], \quad (22)$$

where  $\rho$  is the density of materia,  $P$  is the pressure,  $P_r(\rho)$  is the reference pressure,  $e$  is the specific internal energy per unit mass,  $e_r(\rho)$  is the reference specific internal energy,  $\Gamma$  is a Gruneisen parameter. We choose a simple linear

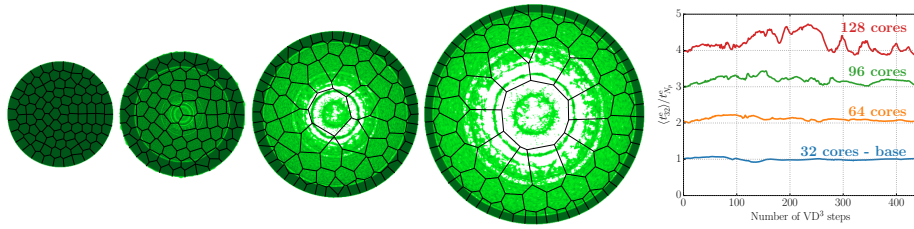


Figure 10: Maps of Voronoi subdomain boundaries and mass distributions during wire explosion simulated with using the VD<sup>3</sup> on 96 processor cores is shown on the left, where the darker blue color corresponds to higher particle density. The relative speedups  $\langle t_{32}^e \rangle / \langle t_{N_p}^e \rangle$  as functions of simulation step in modeling the same problem with 32, 64, 96, and 128 cores are presented on the right. Averaged elapsed time per step in modeling with 32 cores  $\langle t_{32}^e \rangle$  is used for evaluation of the relative speedup.

approximation of the shock Hugoniot in the  $u_s - u_p$  plane, where  $u_s$  is a shock wave velocity and  $u_p$  is a particle velocity behind the shock front :

$$u_s = c_a + s_a u_p, \quad (23)$$

where  $c_a$  and  $s_a$  are fitting parameters, which together with  $\Gamma$  characterize the specific material. Then this relation can be used to derive the reference curves for pressure and internal energy as follows:

$$P_r(x) = \rho_0 c_a^2 \frac{1-x}{[1-s_a(1-x)]^2} \quad (24)$$

$$e_r(x) = \frac{c_a^2}{2} \frac{(1-x)^2}{[1-s_a(1-x)]^2} \quad (25)$$

where  $\rho_0$  is the initial density and  $x = \rho_0/\rho = 1 - u_p/u_s$  is a compression ratio.

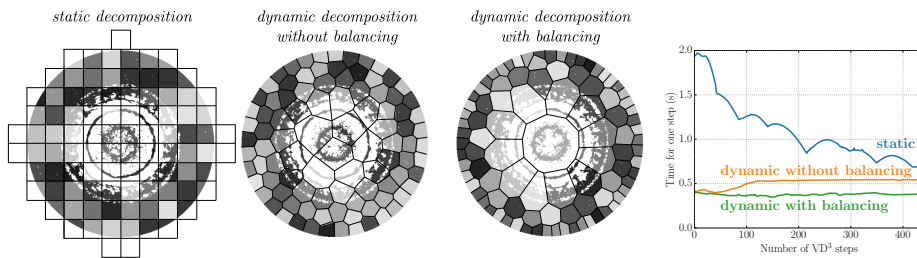


Figure 11: Maps of subdomain boundaries obtained in simulations of wire explosion on 96 cores using the static rectangular decomposition, dynamic Lagrangian without balancing and VD<sup>3</sup> with load balancing, from left to right respectively. Shades of gray are used to distinguish different subdomains only. The right plot shows the corresponding elapsed times per a step during simulation. The areas of Voronoi subdomains become smaller on a liquid cylindrical shell with the highest density to reduce the computational loads in VD<sup>3</sup> with load balancing.

### 5.1. Test 1: ejecta from grooved metal surface

The ejection of a cumulative jet from a shock-loaded grooved metal surface is simulated for a lead sample with a 90-degree opening angle of a groove as illustrated by Fig. 7. The periodic boundary conditions are imposed along the axes  $Oy$  and  $Oz$ . The period (wavelength) of the grooves  $\lambda$  is set to  $40 \mu\text{m}$ ,

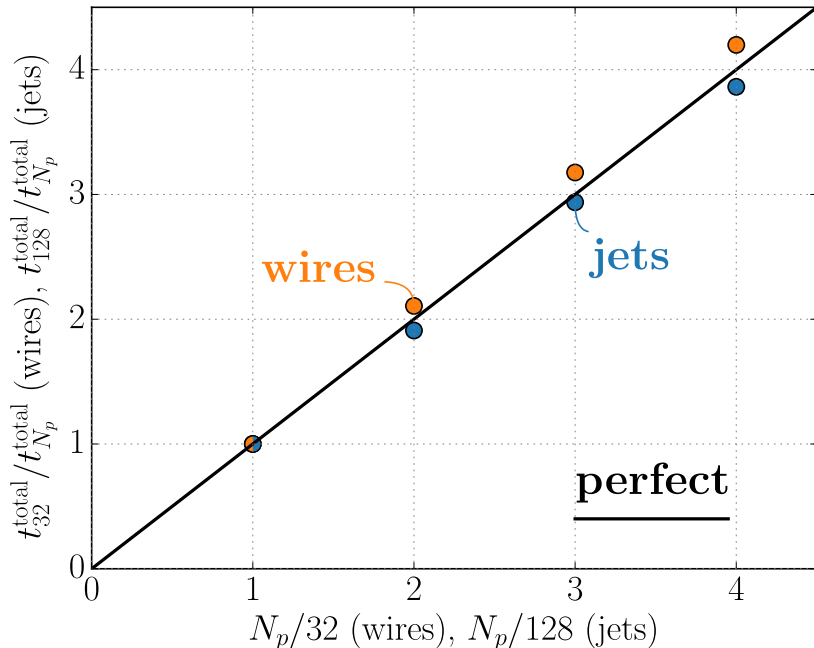


Figure 12: Strong scalability for 1st and 2nd dynamic tests of the load balancing algorithm. Here the wall clock elapsed times  $t_{128}^e$  and  $t_{32}^e$  of entire modeling are chosen as reference values, for the 1st test with ejecta and the 2nd test with wire explosion respectively. The strong scalability is close to a perfect linear speedup in both test, but the 2nd test demonstrates a slightly superlinear speedup because the major part of wire mass happens to be allocated in a thin shell during the explosion, which corresponds to transition from 2D to 1D decomposition for larger numbers of processes  $N_p$  involved.

the sample width is  $2 \mu\text{m}$  along  $z$ , and the length is  $140 \mu\text{m}$ . The size of SPH particles is set to  $0.08 \mu\text{m}$ , so the number of particles in this modeling is 20.8 million. Parameters for the equation of state (22) are:  $\rho_0 = 11.35 \text{ g/cc}$ ,  $c_a = 2.58 \text{ km/s}$ ,  $s_a = 1.26$ , and  $\Gamma = 1.7$ .

Initially, all particles are set to velocity  $u_p = 1 \text{ km/s}$  along the direction  $x$  toward a steady piston in the form of a flat rigid wall. It results in the collision with the piston, which leads to particles stop at the wall and the generation of a shock wave propagating with the velocity of  $u_s - u_p$  in the chosen coordinate system in which the piston/wall is at rest.

Figure 8 shows the evolution of mass distribution with the corresponding Voronoi diagram in simulation on 256 processor cores. During the shock compression, the areas of Voronoi subdomains becomes smaller. The jet formation is accompanied by an inflow of Voronoi subdomains into the jet. During rarefaction, there appear dense and low-density regions in the material sample, which are appropriately covered by the Voronoi diagram. Darker areas with larger numbers of particles are covered by smaller Voronoi subdomains, while the regions with lesser dense material are covered by larger subdomains. The simulation speedup with the increase of processor number remains almost linear despite such variations of mass distribution during the test.

To test the strong scalability, simulations are performed using 128, 256, 384 and 512 processor cores. The plot of the obtained speedup is shown in Fig. 8 on

the right. The wall clock elapsed time required for one simulation step decreases with the increase of the number of processes.

To demonstrate the advantages of dynamic Voronoi decomposition, a comparison with a static domain decomposition is performed as shown in Fig. 9. To do this, 255 subdomains with rectangle shape are placed to cover a large computational domain, which is determined by possible material motion during simulation of ejecta. The initial sample occupies less than half of these steady subdomains, which leads to an increase in the elapsed time required for one simulation step due to uneven distribution of computational loads between processes, see Fig. 9. After formation of a jet and expansion of the sample toward the unoccupied subdomains, the elapsed time per a step decreases. By contrast, both dynamic decompositions with and without load balancing maintain this time per a step at nearly the same level during the entire simulation. But the usage of load balancing results in lesser total simulation time.

It is worth noting that the described algorithm realizes the local load balancing strategy only. In modeling of a system where a large elongation happens, such as in jetting, the connectivity of the individual parts of the diagram decreases to one or two links per a Voronoi subdomain. Then it takes a long time to transfer information about long-range imbalances in the diagram to push additional worker processes to the highly loaded subdomains. As a result, many balancing iterations can be required to establish a global well-balanced decomposition.

To reduce a global load imbalance faster, a global balancing algorithm must be utilized. In particular, the use of a guided flow of Voronoi generators in the direction of an overloaded region makes it possible to improve the load balance in a short time significantly. This approach can also be applied if a large number of particles is created or deleted during the simulation.

### 5.2. Test 2: explosion of aluminum wire

For SPH modeling of an aluminum wire explosion, the following computational setup is used. At the initial time, a cylinder of radius  $R = 6 \mu\text{m}$  and height  $h_z = R/3$  is represented as a set of SPH-particles. Periodic boundary conditions along the  $Oz$  axis are applied. The size of one particle  $d_i$  is set to 40 nm, the total number of particles in the simulation is 3.6 million.

The reference curves which are used in the shock Hugoniot for aluminum (24), are given in accordance with the molecular dynamics data on a sample heated to 4000 K [31]:  $\rho_0 = 1.593 \text{ g/cc}$ ,  $c_a = 3 \text{ km/s}$ ,  $s_a = 1.85$ ,  $\Gamma = 1.5$ . At the initial time, the pressure in the material of the wire is  $P = 2.8 \text{ GPa}$  as a result of the heating. The tensile strength of  $\sigma_c$  in liquid aluminum turned out to be equal to 1.9 GPa, the material density, in this case, is  $\rho = 0.9\rho_0$  according to the results of MD simulation [31].

Figure 10, on the left, shows the process of evolution of the wire during the explosion, calculated using VD<sup>3</sup> on 96 processor cores (1 master process for input-output and 95 workers). At a time  $t > 0$ , a rarefaction wave moves from the cylinder surface to its center (see Fig. 10). During the convergence of the rarefaction wave to the center of the cylinder, the material state exceeds the tensile strength  $\sigma_c$  at 1  $\mu\text{m}$  depth from wire surface. As a result of the explosion, a dense shell forms around the wire, and the internal substance undergoes extreme expansion with cavitation. To simulate this behavior in SPH, pairs of

particles whose density becomes lower than the density at break ( $\rho < 0.9\rho_0$ ) are assumed to be noninteracting, which allows them to form material discontinuities freely.

Initially, all Voronoi subdomains cover equal parts of the wire in terms of the number of particles. During expansion, a region of low density is formed in the central part of the exploding wire, and the balancing algorithm distributes most of the Voronoi subdomains on a dense shell. The inner part of the wire is covered by large Voronoi subdomains in accordance with the low numerical density of the particles.

SPH simulation of this sample was carried out on 32, 64, 96 and 128 processor cores with further calculation of the algorithm acceleration depending on the number of cores used. For all calculations, the system time spent on the SPH integration step is tracked. To calculate the speedup, the reference time is the average time by one step using 32 computational cores. It is shown in Fig. 12 that, if the number of processes is increased, superlinear acceleration is achieved in contrast to the speedup obtained in the 1st test with modeling ejecta.

This can be caused by the two factors: smaller Voronoi subdomains are easier to adapt to an uneven density distribution, and a smaller number of particles ensures better cache hit. The additional acceleration factor is the transition of two-dimensional decomposition into a quasi-one-dimensional decomposition due to the concentration of almost all SPH particles in a thin shell, as indicated in Fig. 10. In this case, the time costs for communication between neighboring Voronoi areas are reduced.

The results of modeling with static and dynamic spatial decomposition into Voronoi domains between CPU cores without load balancing and with balancing on 96 processor cores are presented (see Fig. 11). Static decomposition is a decomposition into rectangular areas covering all the space used by the exploded wire. Turned off load balancing means that  $\Delta\vec{g}_k = 0$  and  $\theta = 0$  in the equations (16), (17), which makes the Voronoi diagram generators only geometric particle centers (6). The time for calculating one simulation step for all decomposition types is shown in Figure 11.

At the beginning of the simulation of wire explosion with static decomposition, only 24 cores are involved. The corresponding time by one step is five times greater than it is for the decomposition in Voronoi cells, where all 95 workers are used at once. During the calculation of wire explosion, SPH particles fill other rectangles in the static decomposition, which results in a more even distribution of the load, so the time for one simulation step decreases. This leads to a decrease in simulation time, which is still greater than it is for the dynamic decomposition. For the case of the dynamic decomposition of generator positions, the Voronoi generators are strictly set to (6) without using the load balancing algorithm ( $\theta = 0$  in (17)). Decomposition without load balancing results in less mobile Voronoi subdomains, which increases the wall clock time of simulation. Dynamic Voronoi decomposition provides a stable time step throughout the simulation due to a more even use of the resources of all processors. Load balancing leads to a better distribution of Voronoi subdomains, providing the shortest time for a single step.

The presented test of the VD<sup>3</sup> algorithm with an exploding wire shows not only better efficiency in comparison with the static decomposition method, but also a linear strong scalability that is demonstrated in Fig. 12. Load balanc-

ing by displacing the generators of the Voronoi diagram is intended to reduce the waiting time for interprocessor communications.

## 6. Conclusion

When using particle methods for modeling phenomena specific for high energy density physics, the variety of particles representing the material samples can evolve from an initially homogeneous distribution (for example, a set of regularly packed particles equal in mass and volume) into a highly heterogeneous one varied in the spatial arrangement and the particle characteristics. The major reasons for such evolution are:

- particle compression in shock waves and expansion in rarefaction waves;
- nonuniform acceleration of material flow by nonplanar compression and rarefaction waves;
- collision between material flows and formation of cumulative jets;
- formation of cavities and free boundaries of complex shape if material is fragmented;
- adaptive merging or splitting of particles to improve the accuracy of modeling.

All listed reasons cause the significant load imbalance and reduce the computational efficiency of parallel modeling of material motion. To address this issue, we have developed the efficient automatic load balancing algorithm for parallel modeling on the large computing clusters with distributed memory. It is based on the spatial dynamic decomposition of simulated samples between Voronoi subdomains, where each subdomain is handled by a single computational process. Voronoi subdomains are allowed to gradually change their shape and position in order to reduce the local imbalance of computational loads via the re-balancing transfer and redistribution of particles between the neighbor processes.

Adaptive load balancing and high computational efficiency are the main advantages of this algorithm. Since the generators of Voronoi subdomains can move freely, the resulting well-balanced Voronoi diagram provides the most computationally attractive coverage for the simulated samples. The evolution of the diagram during simulation is guided by the natural Lagrangian motion of material combined with the load balancing displacements. The algorithm demonstrates fast convergence in static tests of a stationary sample with load imbalance imposed initially and almost linear strong scalability for processor core numbers from tens to several thousand.

Parallel efficiency of our code is illustrated by modeling materials in extreme conditions characterized by large pressure and velocity gradients, at which the spatial distribution of particles can vary greatly in time. In such conditions, our algorithm performs as efficiently as in the static tests and provides the similar strong scalability. The achieved parallel efficiency is superior to that provided by static decomposition algorithm in all dynamic tests.

Our algorithm is recommended to be used in simulations of material samples with essentially dynamic boundaries, flows with large relative velocities, and

particles described by physical models with notably different computational costs, where the automatic balancing with the stable high load of all processes is required during simulation.

## 7. Acknowledgement

This work is supported by the Russian Science Foundation grant 14-19-01599.

## References

- [1] R. A. Gingold, J. J. Monaghan, Smoothed particle hydrodynamics: theory and application to non-spherical stars, *Monthly Notices of the Royal Astronomical Society* 181 (3) (1977) 375–389. doi:[10.1093/mnras/181.3.375](https://doi.org/10.1093/mnras/181.3.375). URL <http://adsabs.harvard.edu/full/1977MNRAS.181..375G>
- [2] A. N. Parshikov, S. A. Medin, Smoothed particle hydrodynamics using interparticle contact algorithms, *Journal of Computational Physics* 180 (1) (2002) 358 – 382. doi:<http://dx.doi.org/10.1006/jcph.2002.7099>. URL <http://www.sciencedirect.com/science/article/pii/S0021999102970993>
- [3] S. Plimpton, Fast parallel algorithms for short-range molecular dynamics, *Journal of Computational Physics* 117 (1) (1995) 1 – 19. doi:<http://dx.doi.org/10.1006/jcph.1995.1039>. URL <http://www.sciencedirect.com/science/article/pii/S002199918571039X>
- [4] R. Murty, D. Okunbor, Efficient parallel algorithms for molecular dynamics simulations, *Parallel Computing* 25 (3) (1999) 217 – 230. doi:[https://doi.org/10.1016/S0167-8191\(98\)00114-8](https://doi.org/10.1016/S0167-8191(98)00114-8). URL <http://www.sciencedirect.com/science/article/pii/S0167819198001148>
- [5] J. W. Shu, B. Wang, M. Chen, J. Z. Wang, W. M. Zheng, Optimization techniques for parallel force-decomposition algorithm in molecular dynamic simulations, *Computer Physics Communications* 154 (2) (2003) 121 – 130. doi:[https://doi.org/10.1016/S0010-4655\(03\)00290-X](https://doi.org/10.1016/S0010-4655(03)00290-X). URL <http://www.sciencedirect.com/science/article/pii/S001046550300290X>
- [6] D. Zhang, C. Jiang, S. Li, A fast adaptive load balancing method for parallel particle-based simulations, *Simulation Modelling Practice and Theory* 17 (6) (2009) 1032 – 1042. doi:<https://doi.org/10.1016/j.simpat.2009.03.003>. URL <http://www.sciencedirect.com/science/article/pii/S1569190X09000355>
- [7] J. Cherfils, G. Pinon, E. Rivoalen, JOSEPHINE: A parallel SPH code for free-surface flows, *Computer Physics Communications* 183 (7) (2012) 1468 – 1480. doi:<https://doi.org/10.1016/j.cpc.2012.02.007>. URL <http://www.sciencedirect.com/science/article/pii/S0010465512000604>



- [8] F. Fleissner, P. Eberhard, Parallel load-balanced simulation for short-range interaction particle methods with hierarchical particle grouping based on orthogonal recursive bisection, *International Journal for Numerical Methods in Engineering* 74 (4) (2008) 531–553. doi:[10.1002/nme.2184](https://doi.org/10.1002/nme.2184). URL <http://dx.doi.org/10.1002/nme.2184>
- [9] I. Sbalzarini, J. Walther, M. Bergdorf, S. Hieber, E. Kotsalis, P. Koumoutsakos, PPM—A highly efficient parallel particle-mesh library for the simulation of continuum systems, *Journal of Computational Physics* 215 (2) (2006) 566 – 588. doi:<https://doi.org/10.1016/j.jcp.2005.11.017>. URL <http://www.sciencedirect.com/science/article/pii/S002199910500505X>
- [10] G. Oger, D. L. Touzé, D. Guibert, M. de Lefte, J. Biddiscombe, J. Soumagne, J.-G. Piccinalli, On distributed memory mpi-based parallelization of SPH codes in massive HPC context, *Computer Physics Communications* 200 (2016) 1 – 14. doi:<https://doi.org/10.1016/j.cpc.2015.08.021>. URL <http://www.sciencedirect.com/science/article/pii/S0010465515003070>
- [11] N. Sato, J. M. Jezequel, Implementing and evaluating an efficient dynamic load-balancer for distributed molecular dynamics simulation, in: *Proceedings 2000. International Workshop on Parallel Processing, 2000*, pp. 277–283. doi:[10.1109/ICPPW.2000.869113](https://doi.org/10.1109/ICPPW.2000.869113).
- [12] A. Ferrari, M. Dumbser, E. F. Toro, A. Armanini, A new 3D parallel SPH scheme for free surface flows, *Computers & Fluids* 38 (6) (2009) 1203 – 1217. doi:<https://doi.org/10.1016/j.compfluid.2008.11.012>. URL <http://www.sciencedirect.com/science/article/pii/S0045793008002284>
- [13] Y. Deng, R. F. Peierls, C. Rivera, An adaptive load balancing method for parallel molecular dynamics simulations, *Journal of Computational Physics* 161 (1) (2000) 250 – 263. doi:<http://dx.doi.org/10.1006/jcph.2000.6501>. URL <http://www.sciencedirect.com/science/article/pii/S002199910096501X>
- [14] C. Begau, G. Sutmann, Adaptive dynamic load-balancing with irregular domain decomposition for particle simulations, *Computer Physics Communications* 190 (2015) 51 – 61. doi:<https://doi.org/10.1016/j.cpc.2015.01.009>. URL <http://www.sciencedirect.com/science/article/pii/S0010465515000181>
- [15] G. Cybenko, Dynamic load balancing for distributed memory multiprocessors, *Journal of Parallel and Distributed Computing* 7 (2) (1989) 279 – 301. doi:[http://dx.doi.org/10.1016/0743-7315\(89\)90021-X](http://dx.doi.org/10.1016/0743-7315(89)90021-X). URL <http://www.sciencedirect.com/science/article/pii/S074373158990021X>
- [16] M. H. Willebeek-LeMair, A. P. Reeves, Strategies for dynamic load balancing on highly parallel computers, *IEEE Trans. Parallel Distrib. Syst.* 4 (9)

- (1993) 979–993. doi:10.1109/71.243526.  
 URL <http://dx.doi.org/10.1109/71.243526>
- [17] Y. F. Hu, R. J. Blake, D. R. Emerson, An optimal migration algorithm for dynamic load balancing, *Concurrency: Practice and Experience* 10 (6) (1998) 467–483. doi:10.1002/(SICI)1096-9128(199805)10:6<467::AID-CPE325>3.0.CO;2-A.  
 URL [http://dx.doi.org/10.1002/\(SICI\)1096-9128\(199805\)10:6<467::AID-CPE325>3.0.CO;2-A](http://dx.doi.org/10.1002/(SICI)1096-9128(199805)10:6<467::AID-CPE325>3.0.CO;2-A)
- [18] V. Zhakhovskii, K. Nishihara, Y. Fukuda, S. Shimojo, T. Akiyama, S. Miyanaga, H. Sone, H. Kobayashi, E. Ito, Y. Seo, M. Tamura, Y. Ueshima, A new dynamical domain decomposition method for parallel molecular dynamics simulation, in: *CCGrid 2005. IEEE International Symposium on Cluster Computing and the Grid, 2005.*, Vol. 2, 2005, pp. 848–854 Vol. 2. doi:10.1109/CCGRID.2005.1558650.
- [19] J.-L. Fattebert, D. Richards, J. Glosli, Dynamic load balancing algorithm for molecular dynamics based on Voronoi cells domain decompositions, *Computer Physics Communications* 183 (12) (2012) 2608 – 2615. doi:<https://doi.org/10.1016/j.cpc.2012.07.013>.  
 URL <http://www.sciencedirect.com/science/article/pii/S0010465512002524>
- [20] L. Fu, X. Y. Hu, N. A. Adams, A physics-motivated Centroidal Voronoi Particle domain decomposition method, *Journal of Computational Physics* 335 (2017) 718 – 735. doi:<http://doi.org/10.1016/j.jcph.2017.01.051>.  
 URL <http://www.sciencedirect.com/science/article/pii/S0021999117300670>
- [21] R. Koradi, M. Billeter, P. Gntert, Point-centered domain decomposition for parallel molecular dynamics simulation, *Computer Physics Communications* 124 (2) (2000) 139 – 147. doi:[http://dx.doi.org/10.1016/S0010-4655\(99\)00436-1](http://dx.doi.org/10.1016/S0010-4655(99)00436-1).  
 URL <http://www.sciencedirect.com/science/article/pii/S0010465599004361>
- [22] X. Zhang, H. Tian, L. Kuo, W. Chen, A contact SPH method with high-order limiters for simulation of inviscid compressible flows, *Communications in Computational Physics* 14 (02) (2013) 425–442. doi:10.4208/cicp.141211.260912a.
- [23] W. Dehnen, H. Aly, Improving convergence in smoothed particle hydrodynamics simulations without pairing instability, *Monthly Notices of the Royal Astronomical Society* 425 (2) (2012) 1068–1082. doi:10.1111/j.1365-2966.2012.21439.x.  
 URL <http://dx.doi.org/10.1111/j.1365-2966.2012.21439.x>
- [24] Q. Du, V. Faber, M. Gunzburger, Centroidal Voronoi tessellations: Applications and algorithms, *SIAM Rev.* 41 (4) (1999) 637–676. doi:10.1137/S0036144599352836.  
 URL <http://dx.doi.org/10.1137/S0036144599352836>

- [25] M. P. Allen, D. J. Tildesley, *Computer Simulation of Liquids*, Clarendon Press, New York, NY, USA, 1987.
- [26] W. Buttler, D. Oró, D. Preston, K. Mikaelian, F. Cherne, R. Hixson, F. Mariam, C. Morris, J. Stone, G. Terrones, D. Tupa, Unstable richtmyer-meshkov growth of solid and liquid metals in vacuum, *Journal of Fluid Mechanics* 703 (2012) 60–84. doi:10.1017/jfm.2012.190.  
URL <https://www.scopus.com/inward/record.uri?eid=2-s2.0-84865504981&doi=10.1017%2fjfm.2012.190&partnerID=40&md5=db1c02196d5cfecce253e5c45f3606ca>
- [27] G. Dimonte, G. Terrones, F. Cherne, P. Ramaprabhu, Ejecta source model based on the nonlinear richtmyer-meshkov instability, *Journal of Applied Physics* 113 (2). doi:10.1063/1.4773575.  
URL <https://www.scopus.com/inward/record.uri?eid=2-s2.0-84872690853&doi=10.1063%2f1.4773575&partnerID=40&md5=818687b964e761e1201701407abd89b4>
- [28] J.-L. Shao, P. Wang, A.-M. He, Microjetting from a grooved al surface under supported and unsupported shocks, *Journal of Applied Physics* 116 (7). doi:10.1063/1.4891733.  
URL <https://www.scopus.com/inward/record.uri?eid=2-s2.0-84906539474&doi=10.1063%2f1.4891733&partnerID=40&md5=003610dc9302831be16df6f0d415413a>
- [29] O. Durand, L. Soulard, Mass-velocity and size-velocity distributions of ejecta cloud from shock-loaded tin surface using atomistic simulations, *Journal of Applied Physics* 117 (16). doi:10.1063/1.4918537.  
URL <https://www.scopus.com/inward/record.uri?eid=2-s2.0-84928570467&doi=10.1063%2f1.4918537&partnerID=40&md5=179cfaa0db0b787385d4598efd32b00e>
- [30] S. I. Tkachenko, A. R. Mingaleev, S. A. Pikuz, V. M. Romanova, T. A. Khattatov, T. A. Shelkovenko, O. G. Ol'khovskaya, V. A. Gasilov, Y. G. Kalinin, Study of the core-corona structure formed during the explosion of an aluminum wire in vacuum, *Plasma Physics Reports* 38 (1) (2012) 1–11. doi:10.1134/S1063780X11120105.  
URL <http://dx.doi.org/10.1134/S1063780X11120105>
- [31] V. V. Zhakhovsky, S. A. Pikuz, S. I. Tkachenko, P. V. Sasorov, T. A. Shelkovenko, P. F. Knapp, C. C. Saylor, D. A. Hammer, Cavitation and formation of foam-like structures inside exploding wires, in: *AIP Conference Proceedings*, Vol. 1426, 2012, pp. 1207–1210. arXiv:<http://aip.scitation.org/doi/pdf/10.1063/1.3686497>, doi:10.1063/1.3686497.  
URL <http://aip.scitation.org/doi/abs/10.1063/1.3686497>